


RESEARCH ARTICLE

Dynamics of N6-methyladenosine modification during aging and their potential roles in the degeneration of intervertebral disc

Libangxi Liu¹ | Hong Sun² | Yang Zhang¹ | Chang Liu¹ | Yong Zhuang² |
Miao Liu² | Xuezheng Ai¹ | Dan Long¹ | Bo Huang¹ | Changqing Li¹ |
Yue Zhou¹ | Shiwu Dong^{3,4} | Chencheng Feng^{1,3} 

¹Department of Orthopaedics, Xinqiao Hospital, Army Medical University, Chongqing, China

²Department of Orthopaedics, Affiliated Hospital of Guizhou Medical University, Guiyang, Guizhou, China

³Department of Biomedical Materials Science, School of Biomedical Engineering, Army Medical University, Chongqing, China

⁴State Key Laboratory of Trauma, Burns and Combined Injury, Army Medical University, Chongqing, China

Correspondence

Chencheng Feng, Department of Orthopaedics, Xinqiao Hospital, Army Medical University, 183 Xinqiao Main Street, Chongqing 400037, China.
Email: doctorfy@163.com

Shiwu Dong, Department of Biomedical Materials Science, School of Biomedical Engineering, Army Medical University, Chongqing, 400038, China.
Email: dongshiwu@tmmu.edu.cn

Yue Zhou, Department of Orthopaedics, Xinqiao Hospital, Army Medical University, 183 Xinqiao Main Street, Chongqing 400037, China.
Email: happyzhou@vip.163.com

Funding information

Natural Science Foundation of Chongqing in China, Grant/Award Numbers: cstc2020jcyj-bshX0091, cstc2019jcyj-msxmX0022; National Natural Science Foundation of China, Grant/Award

Abstract

Background: The N6-methyladenosine (m6A) dynamics in the progression of intervertebral disc (IVD) aging remain largely unknown. This study aimed to explore the distribution and pattern of m6A modification in nucleus pulposus (NP) tissues of rats at different ages.

Methods: Histological staining and MRI were performed to evaluate the degeneration of IVD. The expression of m6A modifiers was analyzed using qRT-PCR and western blot. Subsequently, methylated RNA immunoprecipitation next generation sequencing and RNA-seq were conducted to identify differences in m6A methylome and transcriptome of NP tissues.

Results: Compared to 2-month-old rats, we found significant changes in the global m6A level and the expression of Mettl3 and FTO in NP tissues from 20-month-old rats. During the progression of NP aging, there were 1126 persistently differentially m6A peaks within 931 genes, and 51 persistently differentially expressed genes. GO and KEGG analyses showed that these m6A peaks and m6A modified genes were mainly engaged in the biological processes and pathways of intervertebral disc degeneration (IDD), such as extracellular matrix metabolism, angiogenesis, inflammatory response, mTOR and AMPK signaling pathways. Meanwhile, conjoint analyses and Venn diagram revealed a total of 405 aging related genes contained significant methylation and expression levels in 20-month-old rats in contrast to 2-month-old and 10-month-old rats. Moreover, it was found that four aging related genes with hypermethylated modification including BUB1, CA12, Adamts1, and Adamts4 depicted differentially expressed at protein level, of which BUB1 and CA12 were decreased, while Adamts1 and Adamts4 were increased during the progression of NP aging.

Conclusion: Collectively, this study elucidated the distribution and pattern of m6A modification during the aging of IVD. Furthermore, the m6A modified genes were

Abbreviations: ACAN, aggrecan; BP, biological process; CDS, coding sequence; DEGs, differentially expressed genes; ECM, extracellular matrix; GO, gene ontology; H&E, Hematoxylin and eosin; IDD, intervertebral disc degeneration; IVD, intervertebral disc; KEGG, Kyoto Encyclopedia of Genes and Genomes; m6A, N6-methyladenosine; 2 M, 2-month-old; 10 M, 10-month-old; 20 M, 20-month-old; NP, nucleus pulposus.

Libangxi Liu, Hong Sun, and Yang Zhang have contributed equally to this study.

This is an open access article under the terms of the [Creative Commons Attribution-NonCommercial](https://creativecommons.org/licenses/by-nc/4.0/) License, which permits use, distribution and reproduction in any medium, provided the original work is properly cited and is not used for commercial purposes.

© 2024 The Authors. *JOR Spine* published by Wiley Periodicals LLC on behalf of Orthopaedic Research Society.

Numbers: 81902255, 81972114, 82072495; Special Foundation of Army Military Medical University to enhance scientific and technological innovation ability, Grant/Award Number: 2020XQN15; China Postdoctoral Science Foundation, Grant/Award Number: 2020M673652; Science and Technology Fund of Guizhou Provincial Health Commission, Grant/Award Number: gzwjkj2019-1-133; Basic Research Program of Guizhou Science and Technology Department, Grant/Award Number: QKH-ZK [2022] 430

involved in the IDD related biological processes and pathways. These findings may provide novel insights into the mechanisms and therapies of IDD from the perspective of aging.

KEYWORDS

aging, epigenetic regulation, intervertebral disc degeneration, m6A modification, nucleus pulposus

1 | INTRODUCTION

Intervertebral disc degeneration (IDD) is characterized by nucleus pulposus (NP) herniation, annulus fibrosus rupture, and subsequently nerve roots or dural sac compression or stimulation.¹ IDD, as one of the leading causes of low back and neck pain, has contributed to a great socioeconomic burden for suffers worldwide.² NP serves as a crucial structural component, and is responsible for maintaining the height and biomechanics of intervertebral disc (IVD).³ Increasing studies have shown that loss of number and function of NP cells, and decrease of proteoglycan and water content in NP tissues exacerbate the degeneration of IVD.⁴ It is believed that the degenerative changes in NP tissues account for the major pathogenesis of IDD. Accordingly, maintaining the biological properties and physiological function of NP is vital for prevention and treatment of IDD.^{5–7}

The etiology of IDD is multifactorial, and aging has been found closely associated with the pathogenesis of IDD.⁸ A survey study based on lumbar spine Magnetic resonance imaging (MRIs) has indicated that 40% of subjects under 30 years of age had various degrees of IDD, while the prevalence of IDD progressively raised to over 90% by 50 to 55 years of age.⁹ Hence, IDD is generally considered as an aging related degenerative disease.¹⁰ During the progression of aging, mechanical overloading, nutritional loss, oxidative stress, and dysfunction of genetic and inflammatory factors are found accompanied by the development of IDD.^{11–14} NP cells, as the main type resident in the IVD, gradually become senescence under numerous stimulus of environmental stress and intrinsic factors with age.¹⁵ Senescent NP cells exhibit dysregulated extracellular matrix (ECM) production and cellular functions.¹⁶ Moreover, senescent NP cells aberrantly secrete inflammatory cytokines, matrix proteases, and chemokine, and further affect the normal biological behaviors of neighboring healthy cells.^{15,17} Accumulating evidences have suggested that clearance of senescent cells can alleviate the development of aging related IDD.^{18,19} Thus, inhibiting the senescence of NP cells may be one perspective strategy for the treatment of IDD. However, the underlying mechanisms of NP aging and consequent IDD still remain largely unknown.

Epigenic regulation including DNA methylation, histone modification, noncoding RNAs, and RNA methylation has been demonstrated involving in the pathogenesis of NP cells senescence and aging related IDD.^{20–22} N6-methyladenosine (m6A) is one of the most abundant RNA modifications in mammals.²³ It is well known that m6A modification is the methylation that occurs in the N atom at the sixth position of the adenine.²⁴ M6A modification is a dynamic and reversible process

which is installed by m6A methyltransferases (“writers”), discharged by m6A demethylases (“erasers”), and recognized by reader proteins, thereby participating in regulating the processes of RNA nuclear transport, splicing, stability, translation, and metabolism.²⁵ Multiple studies have suggested that m6A modification implicates in the initiation and progression of diverse diseases via posttranscriptional regulation.²⁶ Recently, several studies have explored the biological functions of m6A modification in the mechanisms of NP cells senescence and aging related IDD.^{20,22,27} All these findings were based on the TNF- α induced senescent model of NP cells and puncture induced animal model of IDD, while no studies have directly investigated the dynamic patterns of m6A during the natural progression of NP aging. Significantly, it was shown that the degeneration level between post-puncture degeneration group and aging degeneration group was different.²⁸ It is reasonable to speculate that a difference of m6A modification patterns may exist between aging and puncture induced IDD model. Hence, deeper insights into the dynamic changes of m6A patterns during the natural aging of NP tissues will help to identify the intrinsic pathogenic factors and further provide novel therapeutic targets for IDD.

Given the fact that epigenetic alterations contribute immensely to aging progression, we hypothesized that the m6A modification during the natural aging of NP tissues is dynamic and may play critical roles in the degeneration of IVD. In this study, we found the global m6A level was significantly increased in aged NP tissues of rats. To further investigate the dynamic patterns of m6A in the aging of rat NP tissues, MeRIP and RNA-seq were adopted to analyze the differentially changed m6A peaks in genes and differentially expressed genes (DEGs), respectively. Conjoint analyses were used to explore the regulation of m6A modification on gene expression. We also conducted gene ontology (GO) and Kyoto Encyclopedia of Genes and Genomes (KEGG) pathway analysis to investigate the biological functions and pathways of m6A modification in the natural progression of NP aging. Altogether, these findings may provide a dynamic landscape of m6A modification, and reveal the potential roles of m6A modification in the process of NP aging and aging related IDD.

2 | MATERIALS AND METHODS

2.1 | Animals

All animal handling and surgical procedures were approved by Animal Ethics Committee of Army Medical University (AMUWEC2020088).

Male Sprague–Dawley (SD) rats with 2-month-old (200 ± 20 g), 10-month-old (450 ± 45 g) and 20-month-old (750 ± 75 g) were purchased from the Animal Center of Army Medical University and each group contained 22 male SD rats fed under specific pathogen-free conditions (12 SD rats for MRI, histology, Western Blot, RNA extraction, and 10 SD rats for MeRIP-seq and RNA-seq). MRI was performed in four rats (Co3/4, 4/5, 5/6) to analyze the degeneration degree of caudal IVDs, and then three rats (Co4/5) were randomly euthanized to obtain paraffin embedded sections of caudal IVDs for histological analysis. NP tissues of all caudal IVDs of eight rats were obtained for western blot and RNA extraction. In another 10 rats, NP tissues of all caudal IVDs was obtained for MeRIP-seq and RNA-seq.

2.2 | Histological analysis

NP tissues were fixed in 4% paraformaldehyde for 2 days, and decalcified for 2 weeks at 37°C in 10% EDTA decalcification solution. After dehydration, the specimens were embedded in paraffin and sectioned into 5- μ m slices. The slices were then deparaffinized and dehydrated, and histological analyzes including Hematoxylin and eosin (H&E) staining, and Safranin O staining were performed according to the manufacture' protocols. We calculated the number of NPCs in each group in nine random fields under 200 \times optical microscope.

2.3 | Magnetic resonance imaging

Rats were anesthetized by inhalation of 4% sevoflurane (Obtained from Daping Hospital noninvasive Surgery Center, Chongqing, China). A magnetic resonance imager (Bruker Pharmascan 7.0 T, Germany) was used to scan the caudal IVDs of the rats, and the parameters were set as follows: TR time: 3000 ms, TE time: 35 ms, incentive time: 7, fat reduction technology: SPAIR, layer thickness: 0.8 mm, and spin echo sequence: TSE sequence. Pfirrmann grading of rat caudal IVDs was calculated according to the Pfirrmann grading criteria of T2-weighted imaging parameters as previously described.²⁹ The degree of IDD was determined in a double-blinded manner according to Pfirrmann grading, NP area and intervertebral height.

2.4 | RNA extraction and qRT-PCR analysis

NP tissue of all caudal IVDs was obtained high-quality RNA for qRT-PCR under in an enzyme-free environment after exposing caudal IVDs according to previously reported methods.³⁰ They should be firstly ground into powder for RNA extraction. Total RNA of NP tissues was extracted using TRIzol reagent (Invitrogen, USA) and RNeasy Mini Kit (Qiagen, Germany). Total RNA was quantitated using a NanoDrop ND-1000 (NanoDrop, Wilmington, DE). qRT-PCR analysis was performed as previously described.³¹ Briefly, a total of 1 μ g RNA was reverse transcribed into cDNA using PrimeScript RT reagent Kit with gDNA Eraser (Takara, Japan). TB Green Premix Ex Taq II (Takara, Japan) was adopted to conduct qRT-PCR amplification with ViiA7 Real-Time PCR system (Thermo Scientific, USA). GAPDH was used as the normalization control. The relative mRNA expression levels were calculated using the $2^{-\Delta\Delta CT}$ method. The primers used in current study are presented in Table 1.

2.5 | Quantitative analysis of global m6A modification

The level of m6A modification in total RNA was detected using Mass Spectrometry. Briefly, adding buffer (500 mM Tris-HCl (aladdin, China), 100 mM NaCl (Sinopharm Chemical Reagent, China), 10 mM MgCl₂ (Bide Pharmatech, China), and 10 mM ZnSO₄ (MACKLIN, USA), pH = 7.0), S1 nuclease (Takara, Japan), Alkaline Phosphatase (Takara, Japan), and Phosphodiesterase I (Sigma, USA) into 1 μ g RNA, and then the mixture was incubated at 37°C. After the RNA was digested into nucleosides completely, the mixture was extracted with chloroform. The resulting aqueous layer was collected for analysis with LC-ESI-MS/MS. The sample extracts were analyzed using an UPLC-ESI-MS/MS system. RNA modifications were analyzed using scheduled multiple reaction monitoring. Data acquisitions were performed using Analyst 1.6.3 software. Multiquant 3.0.3 software was used to quantify all metabolites. Mass spectrometer parameters including the decluttering potentials and collision energies for individual MRM transitions were done with further DP and CE optimization. A specific set of MRM transitions were monitored for each period according to the metabolites

TABLE 1 The primer sequence used in current study.

Target	Primer sequence (5' to 3')	
Mettl3	F: TCGTAACCTATGCTGACCACTCAA	R: CTACCTTCTTGCTCTGCTGTTCTTAG
Mettl14	F: TGGAAAGACTCACTGGAAGCAACTG	R: ACGGCAAGCACTCACATACTCATC
Rbm15	F: TCCTCCTCTTCCTCAGCCACATC	R: GGACGCACCACGGACAATGAT
WTAP	F: AACGGTTGGTCAAGTGTGGCATAT	R: CAGCCTGGTCTACAGAGTGAGTGA
FTO	F: GAGCGGGAAGCTAAGAACTG	R: CTTGTGCAGTGTGAGAAAGGC
ALKBH5	F: TCCTGGAACCTCTGGCTAATCCTGAT	R: ATCTCTACTGGCTACTCTGGTGTGA
GAPDH	F: CGGCAAGTTCAACGGCACAGT	R: CGACATACTCAGCACCAGCATCAC

eluted within this period. The quantification was carried out using a standard curve generated from A and m6A standards ran during the same batch of the samples. The m6A level was calculated as the ratio of m6A to A.

2.6 | Western blot

NP tissue of all caudal IVDs was obtained for western blot under aseptic conditions after exposing caudal IVDs according to previously reported methods.³² Radioimmunoprecipitation assay lysis buffer (P0013, Beyotime, China) was added to collected tissues to extract protein. The protein concentration was measured using a BCA protein assay kit (P0012, Beyotime, China). Electrophoresis and semidry transfer electrophoresis were performed. Equal amounts of total protein (20 µg) of each sample were separated on 5%–12% gradient SDS-PAGE gel (P0012AC, Beyotime) and transferred to a 0.45-µm PVDF membrane (Merck, Germany). After the membrane was blocked by QuickBlock Western blocking solution (P0252, Beyotime, China) for 1 h, and subsequently incubated with different kinds of primary antibodies (Table 2) at 4°C overnight with rotation (the housekeeping proteins used in this study were GAPDH). TBST was used to wash off the unbound antibodies, and then the membranes were incubated with the secondary antibodies of the corresponding species for 1.5 hours and washed again. Then, the membrane was covered with ECL working solution (1705062, Bio-Rad, USA) and incubated for 1–2 min. The membrane was placed in the imaging system for imaging, and Image Lab software was used for analysis of the gray value.

2.7 | MeRIP-seq and RNA-seq

MeRIP-seq and RNA-seq were conducted by LC-Bio Technologies (Hangzhou, China). Briefly, TRIzol (Invitrogen, USA) was used to extract total RNA from NP tissues. The RNA amount and purity of each sample was quantified using NanoDrop ND-1000 (NanoDrop, USA). The RNA integrity was assessed by Bioanalyzer 2100 (Agilent, USA) and confirmed by electrophoresis with

denaturing agarose gel. Dynabeads Oligo (dT) 25-61005 (Thermo Fisher, USA) and Magnesium RNA Fragmentation Module (NEB, USA) were used to purify and fragment Poly (A) RNA. Then the cleaved RNA fragments were incubated with m6A-specific antibody (No. 202003, Synaptic Systems, Germany) in IP buffer to perform m6A RNA immunoprecipitation. Both input samples (all fragments that are not enriched with M6A-modified specific antibodies) without immunoprecipitation and the m6A IP samples (the co-precipitation enriched segment with M6A-modified specific antibodies) were used to construct libraries for MeRIP-seq. The fragmented RNA without immunoprecipitation was also used to generate RNA-seq libraries. Finally, all samples were subjected to 2 × 150 bp paired-end sequencing on an illumina Novaseq 6000.

2.8 | Data analysis

After sequencing, the reads that contained adaptor contamination, low quality bases and undetermined bases with default parameter were removed using fastp software. We found an average of clean data and valid reads was 7.69 Gb and 55.8 million in IP samples as well as 8.71 Gb and 63.8 million in input samples, respectively. The reads of each sample with a sequencing error rate <1% and <0.1% were >97.97% and 94.09%, respectively. More than 96.12% of reads were mapped to the reference genome. Moreover, the unique mapped reads were >72.31% (Table S1). The clean data of all samples were then mapped to the reference genome *Rattus norvegicus* by HISAT2 software. R package exomePeak was used to perform Peak calling analysis, and identify differentially modified genes and changed peaks. Called peaks were annotated by intersection with gene architecture using R package ChIPseeker. The de novo and known motif finding was analyzed by MEME software and HOMER software. The expression level of all genes from input libraries calculated by FPKM was conducted by StringTie software. The differentially expressed genes were selected with log2 (fold change) ≥1 and *p* value <0.05 using R package edgeR. GO and KEGG enrichment analyses were performed based on the differentially changed m6A-modified genes and DEGs.

Primary antibody	Catalog number	Dilution ratio	Source
Mouse anti-GAPDH	60004-1-Ig	WB (1:50000)	Proteintech Group, USA
Rabbit anti-aggrecan	13880-1-AP	WB (1:1000)	Proteintech Group, USA
Rabbit anti-Collagen II	ab188570	WB (1:1000)	Abcam, USA
Rabbit anti-MMP13	18165-1-AP	WB (1:1000)	Proteintech Group, USA
Rabbit anti-Mettl3	15073-1-AP	WB (1:500)	Proteintech Group, USA
Rabbit anti-FTO	27226-1-AP	WB (1:1000)	Proteintech Group, USA
Mouse anti-Bub1	sc-365685	WB (1:500)	Santa Cruz, USA
Rabbit anti-CA12	15180-1-AP	WB (1:1000)	Proteintech Group, USA
Rabbit anti-Adamts1	12749-1-AP	WB (1:500)	Proteintech Group, USA
Rabbit anti-Adamts4	11865-1-AP	WB (1:500)	Proteintech Group, USA

TABLE 2 The primary antibodies used in this study.

2.9 | Statistical analysis

All data were presented as mean \pm SEM from the triplicates of independent experiments and analyzed using GraphPad Prism 9.0 software (La Jolla, CA). ANOVA with Tukey's post-test was used to assess the statistical significance between group means for comparisons among multiple groups. p value <0.05 was considered as statistical significance.

3 | RESULTS

3.1 | Aging related IDD in rat

MRI showed that compared with 2-month-old rats (2 M), Pfirrmann grading of caudal IVD obtained from 10-month-old (10 M) and 20-month-old (20 M) rats was gradually increased, while NP area

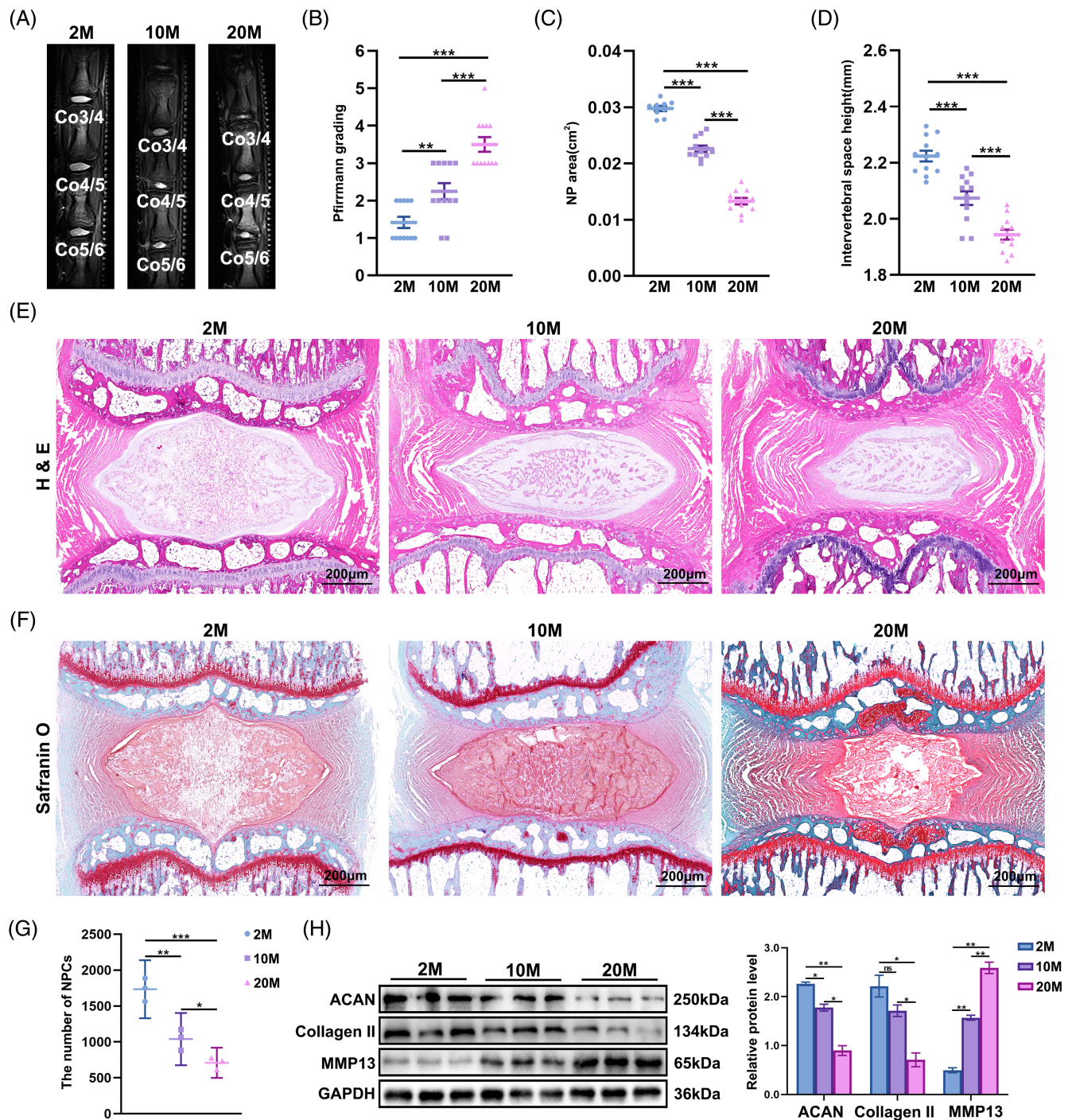


FIGURE 1 Aging related IDD in rats. (A–D) MRI of rat caudal IVDs of different ages. Measurement of Pfirrmann grading, NP tissue area and intervertebral height ($n = 4$, 3 IVDs were detected in each rat, and a total of 12 IVDs were counted). (E) H&E staining of rat caudal IVD sections of different ages. (F) Safranin O staining of rat caudal IVD sections of different ages. (G) The number of NPCs of rat caudal IVDs in different ages ($n = 3$). (H) Western blot and quantification of ACAN, Collagen II and MMP13 in rat NP tissue at different ages ($n = 3$). The data are expressed as the mean \pm SEM, * $p < 0.05$, ** $p < 0.01$, *** $p < 0.001$. ns, no statistical significance; 2 M, 2-month-old; 10 M, 10-month-old; 20 M, 20-month-old.

and intervertebral height were decreased with age (Figure 1A–D). Based on the standardized histopathology of the rat intervertebral disc degeneration model proposed by Lai et al.³³ H&E, and Safranin O staining of caudal IVD showed that the number of NP cells and ECM was decreased gradually, and the large vacuolated NP cells were transformed into clustered and non-vacuolated NP cells with age. In addition, some distorted or disorganized collagen lamellae with minimal (<1/3) infolding of the annulus fibrosus (AF), ruptured or serpentine patterned fibers in <1/3 of the AF and the boundary between the AF and NP gradually became blurred with age. Meanwhile, mild osteophyte or ossification of the endplate appeared with age (Figure 1E–G). Meanwhile, we detected the protein level of biomarkers related to ECM metabolism in NP tissues by western blot. The catabolic enzyme MMP13 was significantly upregulated, while the expression of aggrecan (ACAN) and collagen II, the main components of ECM, was downregulated with age (Figure 1H). Furthermore, the expression of NP senescence markers p18 and p53 increased with age gradually (Figure S1).

3.2 | The global m6A RNA methylation of the IVD is gradually increased with age

We quantified and compared the levels of m6A in total RNA isolated from NP tissues of rats at different ages. Global m6A RNA levels in NP tissues were observed to increase significantly with age (Figure 2A). To investigate whether there were differences in the

expression of modifiers that control m6A modification, we detected “writer” (methyltransferases, including Mettl3, Mettl14, Rbm15, and WTAP) and “erasers” (demethylases, including ALKBH5 and FTO) by qRT-PCR. It was shown that upregulation of Mettl3 and downregulation of FTO were found in NP tissues of 20 M group compared with that in NP tissues of 2 M and 10 M groups at the mRNA levels, while Mettl14, RBM15, WTAP, and ALKBH5 had no significant difference with age (Figure 2B). Furthermore, we examined the protein levels of Mettl3 and FTO in NP tissues of rats at different ages by western blot. It was found that the expression of Mettl3 were increased and the expression of FTO were decreased in NP tissues with age at protein levels (Figure 2C). Taking together, these findings suggested that the expression of m6A modifiers and the level of global m6A RNA methylation in the NP tissues are significantly altered with age.

3.3 | General features of m6A modification in 2 M, 10 M, and 20 M groups

To determine the landscape of m6A modification in the NP aging, we performed MeRIP-Seq to profile the m6A transcriptome in NP tissues across three different time points, including 2, 10, and 20 months. The total m6A peaks were identified by comparing the sequencing data between IP samples and their corresponding input samples. There were 31 986 m6A peaks within 15 166 genes in 2 M group, 32 007 within 15 079 genes in 10 M group, and 19 322 within

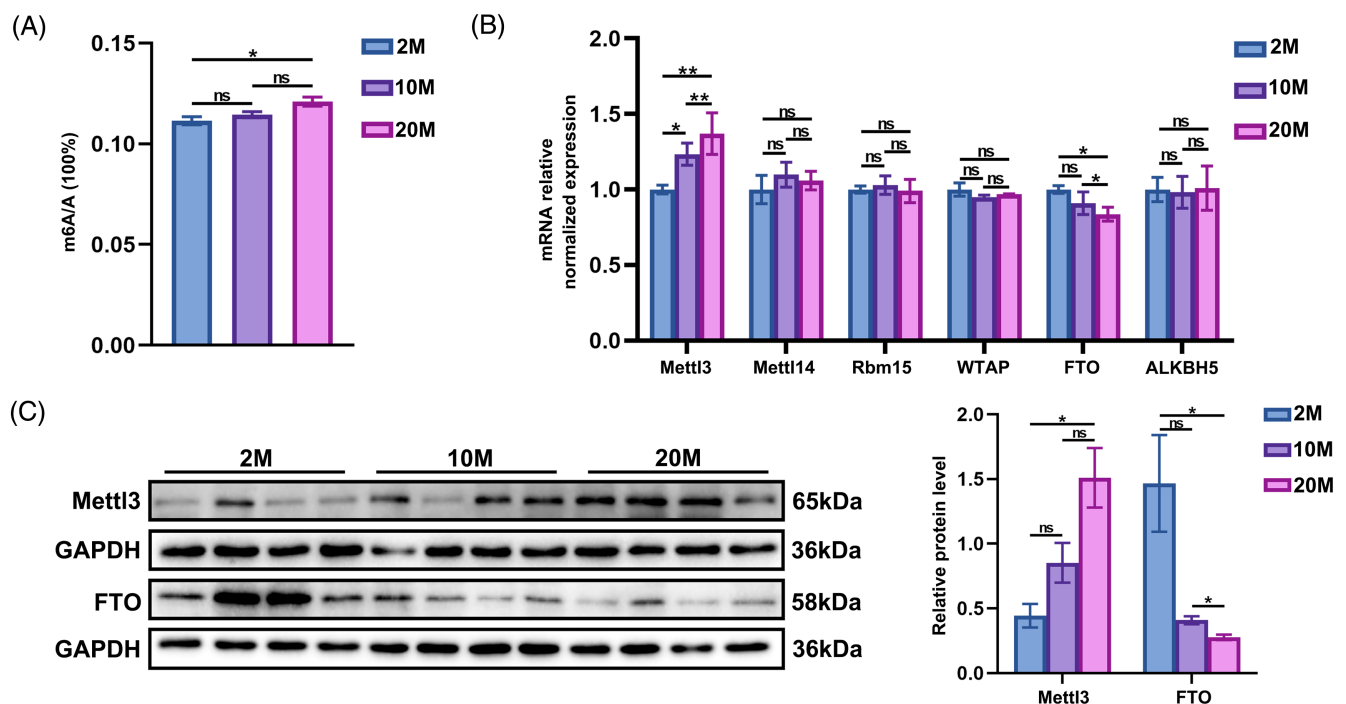


FIGURE 2 The global m6A methylation of the IVD is gradually increased with age. (A) LC-MS/MS quantification of global m6A modification levels in rat NP tissues at different ages ($n = 3$). (B) qRT-PCR of Mettl3, Mettl14, Rbm15, WTAP, ALKBH5 and FTO in rat NP tissue at different ages ($n = 3$). (C) Western blot and quantification of Mettl3 and FTO in rat NP tissue at different ages ($n = 4$). The data are expressed as the mean \pm SEM, * $p < 0.05$, ** $p < 0.01$, *** $p < 0.001$. ns, no statistical significance; 2 M, 2-month-old; 10 M, 10-month-old; 20 M, 20-month-old.

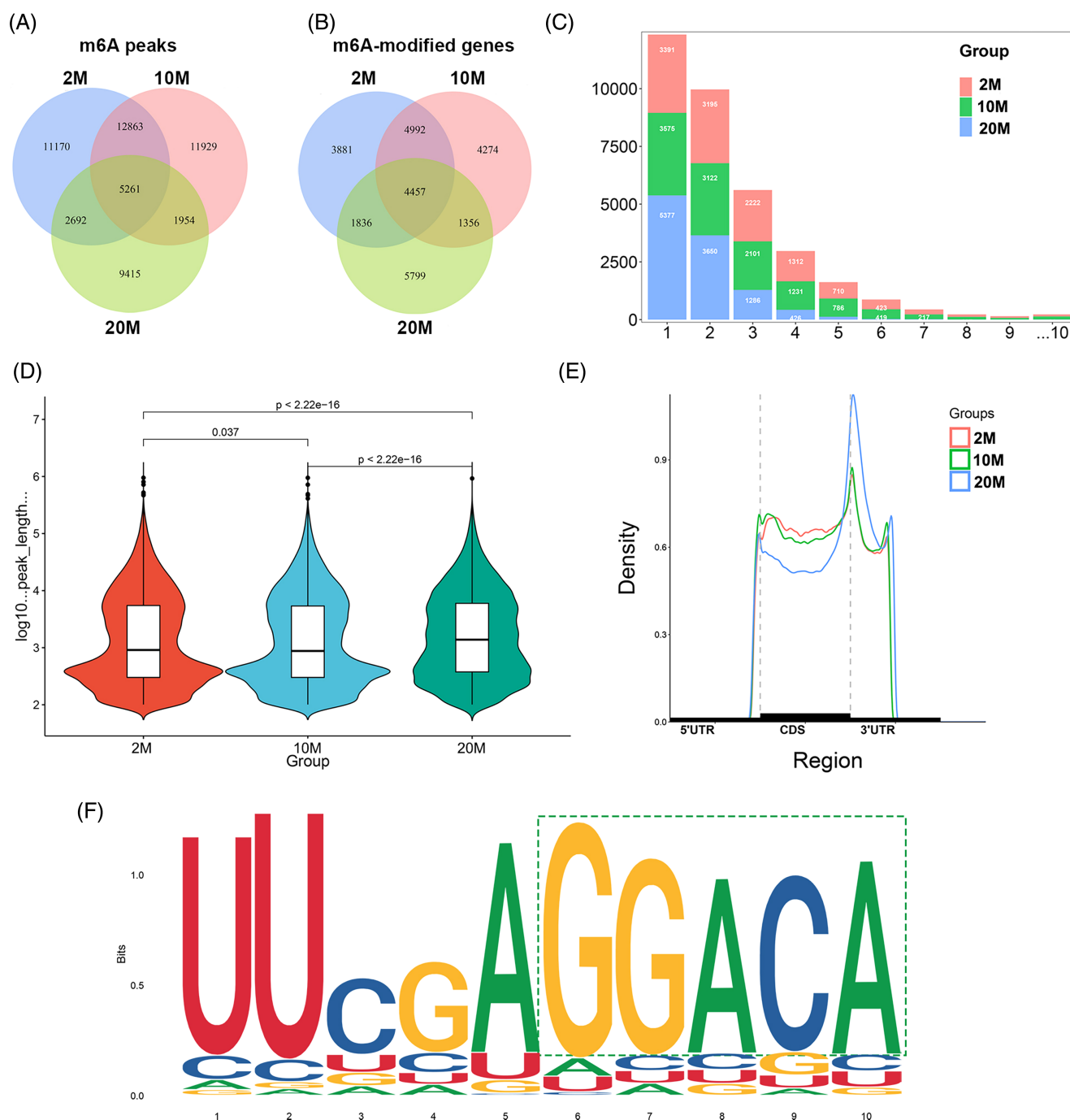


FIGURE 3 General features of m6A modification in 2 M, 10 M, and 20 M groups. (A) Number of m6A peaks in each group. (B) Number of m6A modified genes in each group. (C) Numbers of m6A modified genes with different numbers of m6A peaks. (D) The peak length of each group. (E) The distribution patterns of m6A peaks in gene structure of mRNA. (F) The most conserved sequence motif (RRACH) of three groups.

13 448 genes in 20 M group. Statistics for m6A peaks and m6A-modified genes of each group are shown using Venn diagram (Figure 3A,B). A total of 5261 common m6A peaks and 4457 common methylated genes were found among these three groups, accounting for 9.52% (5261/55284) of the total m6A peaks, and 16.76% (4457/26595) of total m6A-modified genes, respectively. Next, we analyzed the number of m6A peaks per methylated gene, and found that the vast majority of methylated genes (more than 92.05%)

contained <6 m6A peaks (Figure 3C). The average peak length was 7178 bp in 2 M group, 6854 bp in 10 M group, and 7280 bp in 20 M group (Figure 3D). To better understand the preferential locations of m6A peaks, we analyzed the distribution pattern of m6A peaks in the structure of mRNA. The results showed that the m6A peaks were mainly located at regions of the coding sequence (CDS) and 3'UTR (Figure 3E). Moreover, there were some enrichments at the start codon, stop codon, and near the end of 3'UTR (Figure 3E). In addition,

the motif analysis indicated that the most conserved motif sequence was GGACA among these three groups (Figure 3G).

3.4 | Temporal dynamics of m6A modification during NP aging, and functional analysis of persistently differentially m6A-modified genes

To determine the temporal changes of m6A modification during NP aging, we conducted the pairwise comparison of m6A profiles, including 10 M group versus 2 M group (10 M vs. 2 M), and 20 M group versus 10 M group (20 M vs. 10 M). A total of 2406 significantly changed m6A peaks were identified, in which 1483 peaks were up-regulated and 923 peaks were down-regulated in 10 M vs. 2 M. The top 20 significantly changed m6A peaks in 10 M vs. 2 M is shown in Table S2. As shown in Figure S2A, the peaks with significant changes were mainly located in the CDS (42%), 3'UTR (22.7%), and stop codon (21.3%). Meanwhile, a total of 2073 genes were found with differentially changed m6A peaks (Figure S2B). GO and KEGG analyses were performed to elucidate the biological functions and pathways of differentially methylated genes in 10 M vs. 2 M (Figure S2C,D). Meanwhile, a total of 16 025 significantly altered m6A peaks were distinguished, in which 13 775 peaks increased and 2250 peaks decreased in 20 M vs. 10 M. The top 20 significantly changed m6A peaks in 20 M vs. 10 M is shown in Table S3. Similar to the 10 M vs. 2 M, the peaks with significant changes in 20 M vs. 10 M comparison were mostly distributed in the CDS (31.5%), followed by stop codon (30.1%), and 3'UTR (21.5%) (Figure S2A). Interestingly, we observed 10 463 genes that were marked with m6A modification (Figure S2E). Both the number of m6A peaks and methylated genes showed significant increases in 20 M vs. 10 M when compared to that in 10 M vs. 2 M. The top 20 GO and KEGG categories are shown in Figure S2F,G.

To further functional insights into m6A modification in the NP aging, we screened the m6A peaks with persistent difference at different ages of NP tissues. As shown in Table S4, a total of 1126 persistently differentially changed m6A peaks within 931 genes were identified among these three groups, in which 981 peaks within 802 genes were found upregulated and 145 peaks within 128 genes were found downregulated. Subsequently, GO and KEGG analyses were performed to clarify the biological functions and pathways of persistently differentially methylated genes. Overall, the persistently hypermethylated genes were mainly enriched in protein processing, microtubule-based movement, and regulation of transcription, whereas the persistently hypomethylated genes were mostly involved in peptide metabolic process, cytoskeleton-dependent intracellular transport, and negative regulation of blood vessel endothelial cell migration in terms of biological process (BP) categories (Figure 4A,B). KEGG analyses indicated that the persistently hypermethylated genes were mainly enriched in mTOR signaling pathway, autophagy, and AMPK signaling pathway, while persistently hypomethylated genes were mostly associated with RNA degradation, TNF signaling pathway, and apoptosis (Figure 4C,D). Furthermore, two

representative genes with persistently altered peaks were selected to illustrate the m6A modified pattern in the structure of mRNA. The peaks of *Plce1* were located at the regions of 5'UTR and 3'UTR, and the peaks of *Scd* were located at the regions of 5'UTR, CDS, and 3'UTR (Figure 4E,F).

3.5 | Overview of genes expression profiles in 2 M, 10 M, and 20 M groups

In order to further explore the potential relationship between the degree of m6A modification and gene expression, we investigated the differences of gene expression among groups using the RNA sequencing data of input samples. It was shown that a total of 175 genes were up-regulated while 156 genes were down-regulated in 10 M vs. 2 M (Table S5 and Figure S3A,B). The top 20 GO and KEGG terms are listed in Figure S3C,D. Remarkably, the enriched KEGG pathways were related to the progression of aging and IDD, such as PI3K-Akt signaling pathway,³⁴ MAPK signaling pathway,³⁵ and NF- κ B signaling pathway.^{4,34} Besides, there were 625 genes increased and 307 genes decreased in 20 M vs. 10 M (Table S6 and Figure S4A,B). The top 20 GO and KEGG categories are exhibited in Figure S4C,D. The differentially expressed genes were mainly involved in aging and oxidative stress, such as p53 signaling pathway,³⁶ and FOXO signaling pathway.³⁷

Next, we also analyzed the persistently DEGs at different stages of IVD. As shown in Table S7, a total of 51 genes were found persistently differentially expressed among groups, in which 28 genes were up-regulated and 23 genes were down-regulated. GO analyses revealed that the persistently upregulated genes were mainly enriched in negative regulation of transcription involved in meiotic cell cycle, inflammatory response, and negative regulation of angiogenesis, whereas the persistently downregulated genes were mostly involved in negative regulation of ECM assembly, regulation of IL-1 β production, and positive regulation of metalloproteinase activity in terms of BP categories (Figure 5A,B). KEGG analyses showed that the persistently upregulated genes were mainly enriched in TGF- β signaling pathway, p53 signaling pathway, and PI3K-Akt signaling pathway, while the persistently downregulated genes were mostly associated with NOD-like receptor signaling pathway, Jak-STAT signaling pathway, and Estrogen signaling pathway (Figure 5C,D).

3.6 | Identification the regulation pattern of m6A modification and gene expression during NP aging though combined analysis

It is believed that m6A modifications function as important regulators in gene expression.³⁸ Hence, a combined analysis between MeRIP-seq and RNA-seq was performed to identify the regulation pattern of m6A modification in aging related genes of IVD, and the results were described using a four-quadrant diagram. In the comparison of 20 M group versus 2 M group (20 M vs. 2 M), there were 21 genes with

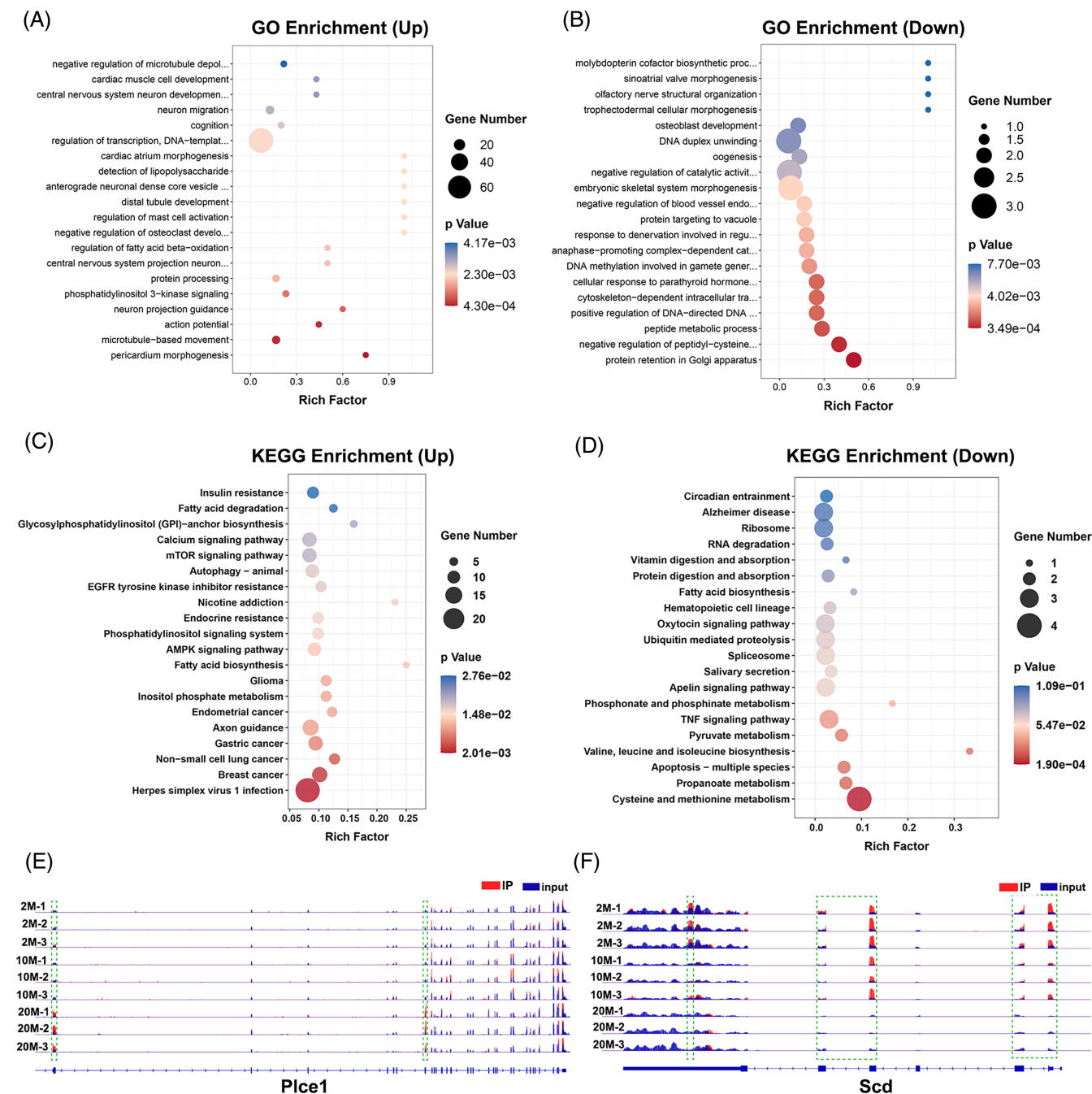


FIGURE 4 Functional analyses of persistently differentially m6A-modified genes. (A) The top 20 enriched GO terms of persistently upregulated m6A-modified genes. (B) The top 20 enriched GO terms of persistently downregulated m6A-modified genes. (C) The top 20 enriched pathways of persistently upregulated m6A-modified genes. (D) The top 20 enriched pathways of persistently downregulated m6A-modified genes. (E-F) Visualization of two representative genes with persistently differently changed peaks during NP aging, including Plce1(E) and Scd (F).

hypomethylation and upregulated expression (hypo-up), 315 genes with hypermethylation and upregulated expression (hyper-up), 72 genes with hypomethylation and downregulated expression (hypo-down), and 659 genes with hypermethylation and downregulated expression (hyper-down) (Figure 6A and Table S8). In 20 M vs. 10 M, there were 21 genes with hypomethylation and upregulated expression, 134 genes with hypermethylation and upregulated expression, 58 genes with hypomethylation and downregulated expression, and 426 genes with hypermethylation and downregulated expression

(Figure 6B and Table S9). Furthermore, Venn diagram analysis was conducted to screen the specific genes associated with aging, and clarify the regulation pattern of m6A modification. We observed a total of 90 genes both increased in m6A modification and gene expression, and a total of 18 genes decreased in both m6A modification and gene expression. Besides, there were 295 genes with hypermethylation and downregulated gene expression, and two genes with hypomethylation and upregulated gene expression (Figure 6C and Table S10).

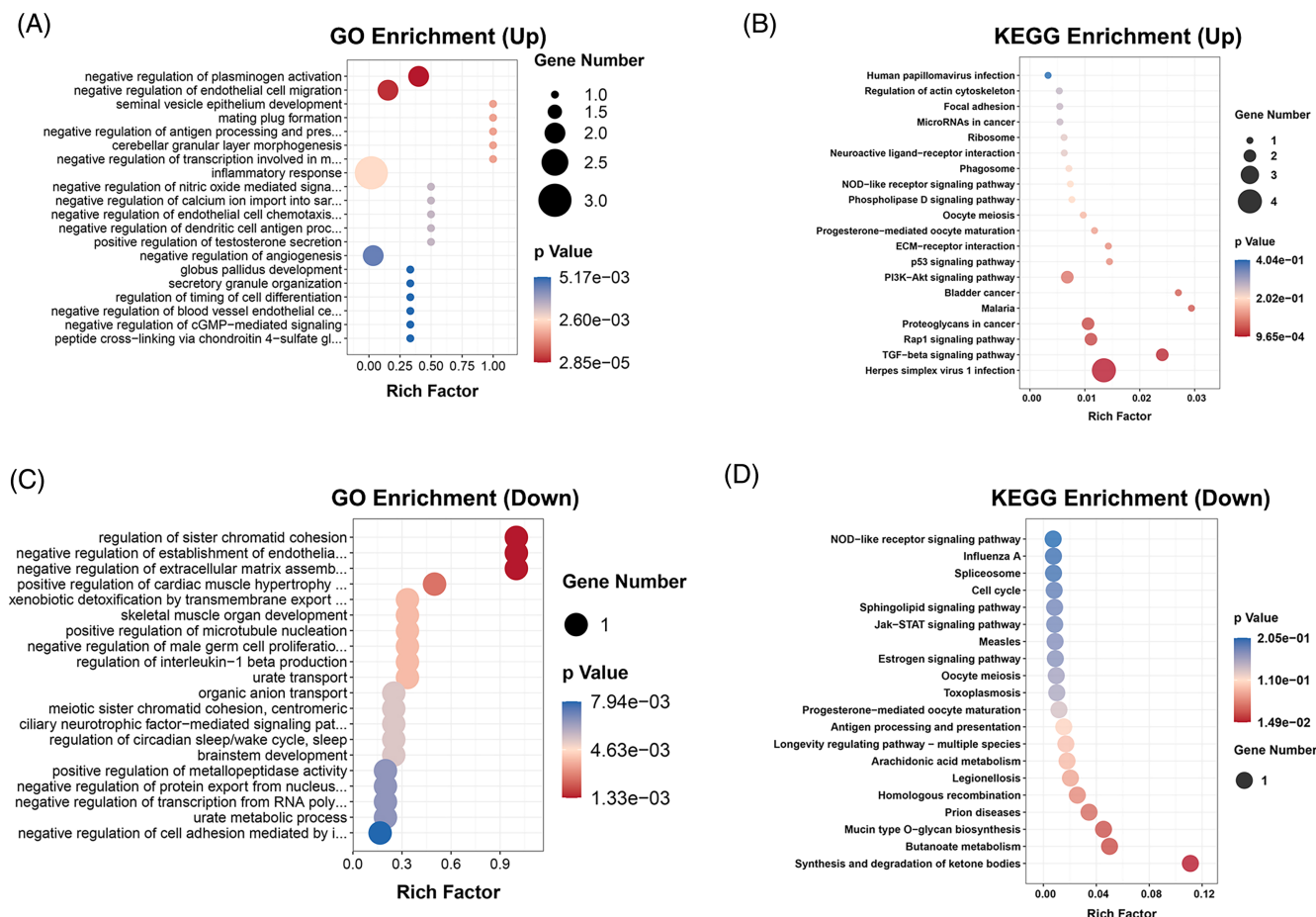


FIGURE 5 Functional analyses of persistently differentially expressed genes. (A) The top 20 enriched GO terms of persistently upregulated genes. (B) The top 20 enriched pathways of persistently upregulated genes. (C) The top 20 enriched GO terms of persistently downregulated genes. (D) The top 20 enriched pathways of persistently downregulated genes.

As the m6A content of total RNA was significantly enhanced during the progression of NP aging (Figure 1A), we chose those genes with hypermethylated modification for further analysis. Though GO analyses, we found those genes with hypermethylation and upregulated gene expression were chiefly enriched in response to anoxia, reactive oxygen species metabolic process, and regulation of transcription, whereas those genes with hypermethylation and downregulated gene expression were engaged in acrosomal vesicle exocytosis, secretion of lysosomal enzymes, and positive regulation of acute inflammatory response (Figure 6D,E). KEGG analyses indicated that those genes with hypermethylation and up-regulated genes expression were mainly associated with FOXO signaling pathway, PI3K-Akt signaling pathway, and ribosome, whereas those genes with hypermethylation and downregulated genes expression were involved in RIG-I-like receptor signaling pathway, oxidative phosphorylation, and NOD-like receptor signaling pathway (Figure 6F,G).

3.7 | Validation and qualification of candidate aging related genes

Four aging related genes including BUB1, CA12, Adamts1, and Adamts4 have been reported closely associated with the pathogenesis

of IDD.^{39–41} The combined analysis of MeRIP and RNA-seq showed that the m6A modification level of BUB1 and CA12 was increased while the expression was decreased, and the m6A modification level and expression of Adamts1 and Adamts4 were both increased with age. Results from the IGV genome browser demonstrated that the m6A modification level of the BUB1, CA12, Adamts1, and Adamts4 were remarkably higher in NP tissues of aged IVD (Figure 7A–D). Western blot showed that the expressions of BUB1 and CA12 were significantly decreased, while the expressions of Adamts1 and Adamts4 were significantly increased with age (Figure 7E), which were consistent with the results identified from RNA-seq.

4 | DISCUSSION

IDD is a multifactorial disease with a high incidence, and the caused symptoms seriously affect the daily life of patients. An increasing number of studies have focused on the potential function and mechanism of m6A modification in IDD.⁴² However, no study has described the landscape of m6A changes in aging related IDD yet. In this study, IVD tissues were obtained from different ages of rats, and the degenerative changes were verified through MRI scanning, histological staining, and western blot. Moreover, it was found that the levels of global

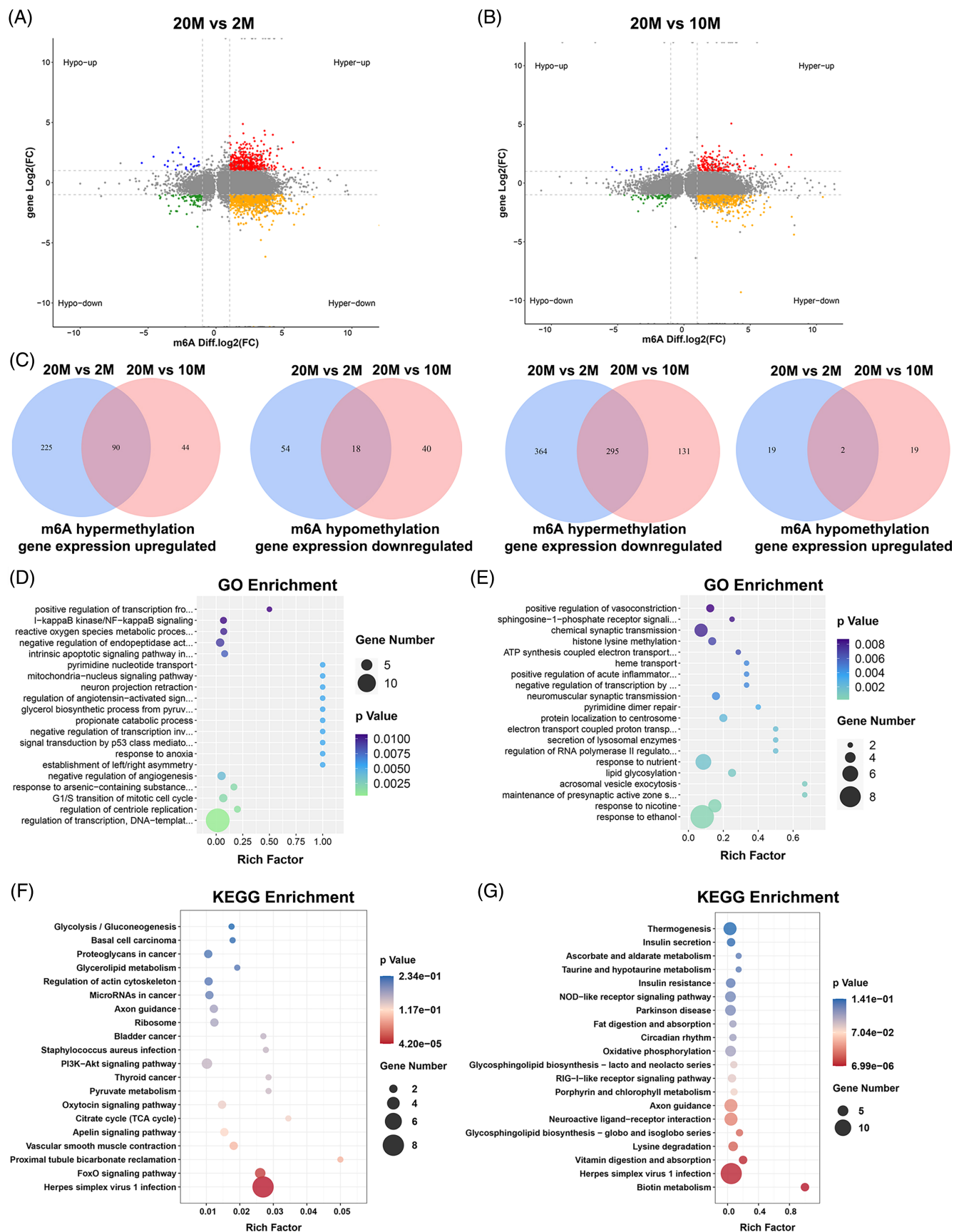


FIGURE 6 Legend on next page.

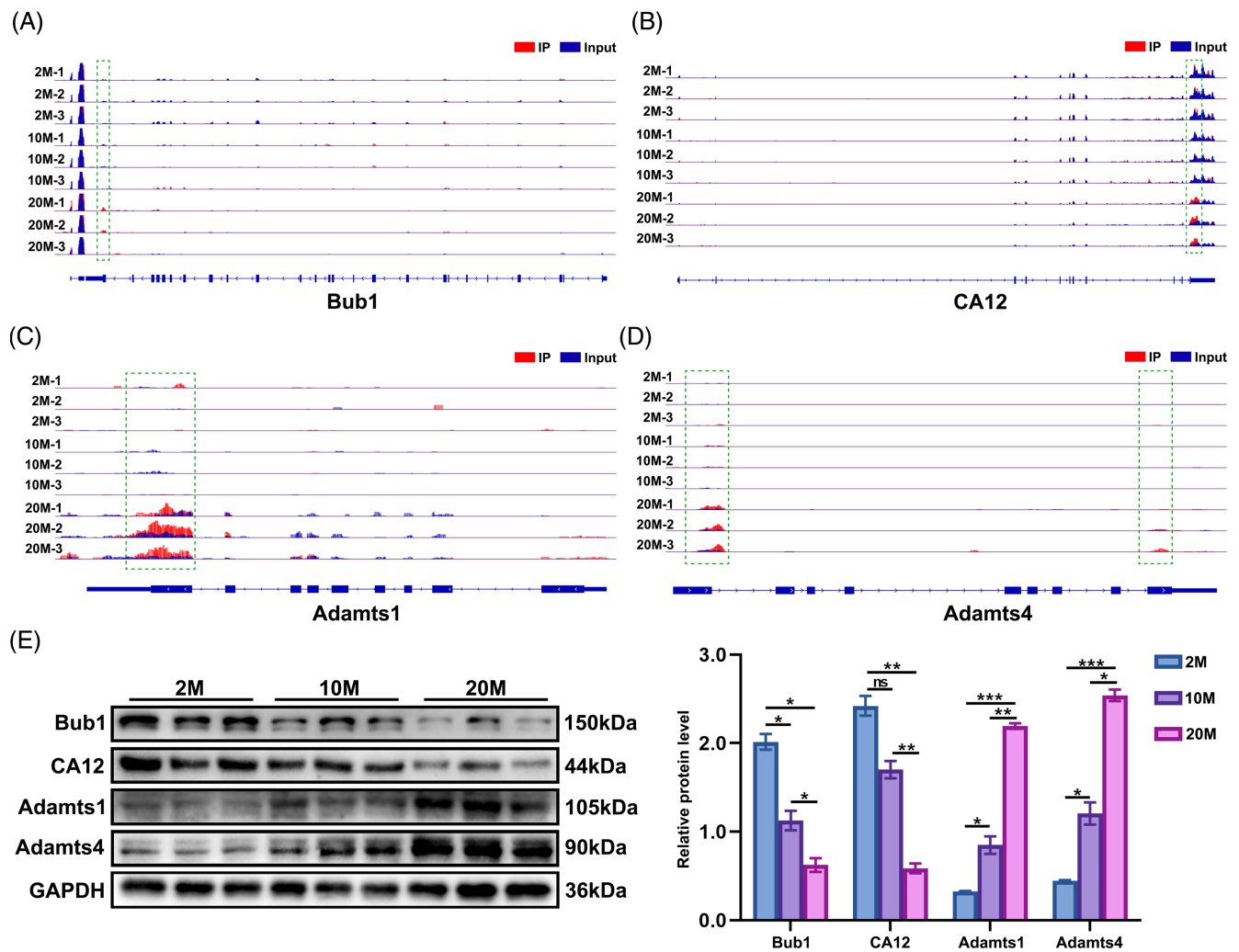


FIGURE 7 Validation and qualification of candidate aging m6A-modified genes. (A-D) Peak distribution of Bub1(A), CA12 (B), Adamts1(C) and Adamts4 (D) in rat NP tissues at different ages in IGV genome browser ($n = 3$). (E) Western blot and quantification of Bub1, CA12, Adamts1 and Adamts4 in rat NP tissues at different ages ($n = 3$). The data are expressed as the mean \pm SEM, * $p < 0.05$, ** $p < 0.01$, *** $p < 0.001$, ns, no statistical significance; 2 M, 2-month-old; 10 M, 10-month-old; 20 M, 20-month-old.

m6A modification and m6A modifiers including Mettl3 and FTO were significantly altered in aged NP tissues. In addition, MeRIP-seq and RNA-seq were performed to identify m6A peaks and m6A-modified genes in NP tissues of rats at different ages. It was found that heterogeneity of m6A modifications in NP tissues existed at different ages of rats. These findings indicated that the differential changes of m6A modification in NP tissues appear to be closely associated with the

occurrence and development of aging related IDD. Deeper insight into these m6A changes may shed new light on the underlying mechanisms of IDD, and thus provide novel therapeutic targets for degenerative disc related diseases.

The IVD, a kind of heterogenous tissue, lies between adjacent vertebral bodies, which is account for flexibility and load support of spine in mammals. The etiologies of IDD remain quite complicated.

FIGURE 6 Identification the regulation pattern of m6A modification and gene expression during NP aging though combined analysis. (A) Four-quadrant graph exhibits the DEGs containing differentially changed peaks in 20 M vs. 2 M. Conjoint analyses of differentially changed peaks and DEGs resulted in four groups of genes: hypomethylated and upregulated genes (hypo-up), hypermethylated and upregulated genes (hyper-up), hypomethylated and downregulated genes (hypo-down), hypermethylated and downregulated genes (hyper-down). (B) Four-quadrant graph shows the DEGs containing differentially changed peaks in 20 M vs. 10 M. (C) Identification of aging related m6A-modified genes between 20 M vs. 10 M and 20 M vs. 2 M. (D) The top 20 enriched GO terms of genes with hypermethylation and upregulated gene expression. (E) The top 20 enriched GO terms of genes with hypermethylation and downregulated gene expression. (F) The top 20 enriched pathways of genes with hypermethylation and upregulated gene expression. (G) The top 20 enriched pathways of genes with hypermethylation and downregulated gene expression.

Mechanical, traumatic, genetic and nutritional factors can contribute to the progression of IDD.⁴³ Significantly, aging is considered as one of important factors leading to the pathogenesis of IDD.⁴⁴ The aging related degeneration can lead to structural lesions, and disorder of ECM metabolism. As shown in our study, the NP area and intervertebral height of caudal IVD were decreased in 10- and 20-month-old rats followed by increased Pfirrmann MRI grading when compared to that in 2-month-old rats. Meanwhile, histological experiments showed that the number of NP cells and NP constitutes of IVDs area was decreased gradually. The large vacuolated NP cells were transformed into clustered and non-vacuolated NP cells with age. And the boundary between the AF and NP gradually became blurred with age. In addition, distorted or disorganized collagen lamellae gradually appears in AF, as well as fiber ruptured or serpentine patterns with age. Furthermore, mild osteophyte or ossification of the endplate appeared with age. Moreover, we found that anabolic makers including collagen II, and aggrecan were downregulated, whereas the catabolic marker such as MMP13 was upregulated in the NP tissues of 10- and 20-month-old rats in contrast to 2-month-old rats. NP is known as the main component of IVD. The changes in structure of IVD and the abnormal metabolism of ECM may be attributed to the alternation in the molecular phenotype of NP cells during NP aging.^{15,45} Hence, further investigation into the aged NP tissues and cells will help elucidate the molecular mechanisms of IDD.

Increasing studies have indicated that m6A modification occurs in TNF- α induced senescent model, puncture induced animal models, and also human IDD.^{11,20,22} Although m6A modification plays important roles in the progression of these cell and animal models, some differences of m6A patterns exist among these models in published studies. It is shown that m6A modification is regulated dynamically by multiple methyltransferases and demethylases, such as Mettl3, Mettl14, WATP, FTO, and ALKBH5.²⁶ Recent evidences have indicated that several m6A modifiers can function as critical factors in the progression of IDD.⁴² As the main components of methyltransferases, Mettl14 can form a heterodimer with Mettl3 to catalyze m6A methylation. Zhu et al. have confirmed that Mettl14 expression was positively correlated to m6A level in human NP cells, and Mettl14 knockdown could rescue the TNF α induced cell senescence.⁴⁶ Moreover, Mettl14 was able to stabilize NLRP3 mRNA and thus promote its expression. Consequently, the elevated NLRP3 increased the proinflammatory factors including IL-1 β and IL-18, therefore triggering pyroptosis of NP cells.⁴⁷ Mettl16 was found upregulated in the degenerative NP tissues. Overexpression of Mettl16 could aggravate oxidative stress induced apoptosis of NP cells by disturbing the balance of splicing, maturation, and degradation of MAT2A pre-mRNA though m6A manner.¹¹ ALKBH is one of main m6A demethylases. A previous study verified that ALKBH5 was upregulated during IVD denegation and NP cell senescence. Consequently, ALKBH5 demethylated DNMT3B transcripts and thus enhanced its expression, thereby promoting the progression of IVD degeneration and NP cell senescence.²⁰ In addition, Mettl3 expression and m6A methylation level have been found significantly increased in degenerative human endplate cartilage tissues. Mettl3-mediated m6A methylation could

accelerate tension stimulation caused SOX9 downregulation, thereby inhibiting the synthesis of ECM in endplate chondrocytes.⁴⁸ There may inevitably be some differences between these models in the regulation of specific genes and biological processes by m6A modification. These findings from current study need to be further investigated in order to better reveal and fit the mechanisms of human IDD. In our study, Mettl3 was upregulated while FTO was downregulated gradually in NP tissues of rats with age, which was consistent with the results obtained from a standing mouse model.⁴⁹ However, no significant difference was found in the expression of Mettl14, Rbm15, WTAP, and ALKBH5. It is well established that the total m6A level is determined by the dynamical balance of methyltransferases and demethylases.²⁶ Hence, we speculated that the upregulation of total m6A level during the progression of NP aging was attributed to the increase of Mettl3 and the decrease of FTO. Interestingly, Castro-Hernández et al demonstrated a decreased m6A level of brain tissues in aged animals and Alzheimer's disease patients.⁵⁰ Moreover, a lower level of m6A modification was also detected in the striatum of rat brain undergoing Parkinson's disease.⁵¹ The discrepancies of m6A modification between IDD and neurodegenerative diseases indicate that the level of m6A modification during aging may vary from species, organs, and diseases.

With the development of MeRIP-seq, more details about m6A modification in NP tissues of IDD have been carried out. Zhu et al have identified the landscape and distribution patterns of m6A modification in NP tissues from a standing mouse model.⁴⁹ The results showed that there were 19 742 peaks within 8796 genes, and 17846 peaks within 8173 genes in normal control and standing mouse model, respectively. Meanwhile, a total of 1319 m6A peaks with significant changes were characterized, in which 933 were upregulated, and 386 were downregulated. In our study, we performed MeRIP-seq to identify m6A changes in NP tissues at different ages of rats, and found that the number of m6A peaks was 31 986, 32 007, and 19 322 in 2-month-old, 10-month-old, and 20-month-old rats, respectively. The most consensus motif sequence among these three groups was GGACA, similar to the observation in other aged mammals, such as human,⁵⁰ and mouse.⁵² On one level, this resemblance may elucidate the conserved features of m6A modification in mammals during the progression of aging. As for the distribution of m6A peaks, they were mainly enriched in the region of CDS and 3'UTR. Notably, the peaks with significant changes of CDS in 20 M vs. 10 M were markedly decreased when compared to that in 10 M vs. 2 M, whereas the peaks with significant changes in stop codon were increased, which may indicate that aging related factors mainly contribute to the m6A changes at the regions of CDS and stop codon. Moreover, our results showed that the genes with the differentially changed m6A modification were mainly in charge of RNA degradation, RNA transport, protein phosphorylation and ubiquitination, and protein binding. These findings may be due to the abundant m6A modifications at CDS and 3'UTR, which are responsible for the RNA stability, transport, and protein synthesis.^{25,53,54}

A large number of studies have suggested that m6A modification is relevant to aging related processes and diseases, such as oxidative

stress, DNA damage, cell senescence, autophagy, neurodegenerative diseases, diabetes, and cardiovascular diseases.⁵⁵ Genes with differentially changed m6A modification have been proved responsible for the regulation of these biological processes and diseases.^{56–58} There is little known regarding the biological functions of m6A-modified genes in the aging related IDD. In order to further investigate the role of m6A modification in the progression of aging, genes with persistent methylation were screened among these three groups. Interestingly, a total of 931 genes showed persistently methylated trends during the progression of NP aging. GO analyses showed that these genes with persistently methylated trends were mainly associated with the metabolism of protein and lipid, RNA biosynthesis, and angiogenesis, indicating that the persistently changed m6A peaks may play critical roles in the abnormal metabolism during the development of IDD.^{59,60} Regarding the pathway analysis, these genes with persistently methylated trends were primarily engaged in cell death and inflammation related pathways, such as mTOR signaling pathway, and AMPK signaling pathway.^{61,62} A majority of studies have demonstrated that systemic chronic inflammation is accompanied by the progression of aging, thereby participating the occurrence of cellular senescence, immunosenescence, organ dysfunction, and aging related diseases.⁶³ Significantly, mTOR signaling pathway, and AMPK signaling pathway have been demonstrated to the aging and degeneration of IVD.^{64,65} Inhibition of mTOR complex 1 attenuated inflammation induced disc cellular apoptosis, senescence, and ECM degradation, through activation of autophagy and Akt-signaling network.⁶⁶ Activation of AMPK signaling pathway could reduce the expression of Col2a1, ACAN, and DCN, accompanied with the induction of NP apoptosis and senescence.⁶⁷ Hence, regulation of mTOR and AMPK signaling pathways via the m6A-dependent manner may be prospective targets for preventing aging related IDD.

The significance of m6A modification in multiple biological processes has been demonstrated mainly attributed to the post-transcriptional regulation of gene expression.^{26,38,54} In order better understanding the roles of m6A modification in the regulation of aging related genes, we screened the genes with differentially changed peaks and differential expression in 20 M group in comparison to 10 M and 2 M groups. We found 405 genes whose m6A peaks and mRNA levels both changed significantly. Consistent with the expression trends of Mettl3 and FTO during the progression of NP aging, the number of genes with hypermethylation were more than that with hypomethylation. Previous studies have demonstrated that one of the main functions of m6A modification is to facilitate mRNA degradation, indicating a negative relationship between m6A modification and gene expression.^{26,68} In present study, most of aging related genes contained opposite trends between m6A modification and gene expression. For instance, BUB1 and CA12 were found persistently hypermethylated, and the results of western blot showed their expression was downregulated during the progression of NP aging. Significantly, less than one third of aging related genes exhibited a positive correlation between m6A modification and gene expression. For instance, Adamts1 and Adamts4, as the major catabolic enzymes in IVD tissues, were observed with persistent hypermethylation among groups. Meanwhile, the expression of Adamts1 and Adamts4

was increased with age. These distinctions of m6A modification mediated post-transcriptional regulation may be due to the different functions of m6A “readers”, of which YTHDF1 and YTHDF2 have been found accelerating mRNA degradation,^{69,70} whereas IGF2BP2 could promote mRNA stability and translation.^{71–73} Thus, the effect of m6A modification on the expression of exact genes remains to be further clarified.

However, some limitations should be interpreted in current study. First, as any animal model has limitations, this study was only conducted with NP tissue of male SD rats caudal IVDs. Considering that the gender of the rats and the composition and structure of the IVDs may bias the experimental results, further study the m6A modification changes in NP, AF and CEP of male and female rats will provide a global view in understanding the relationship between m6A modification and aging-related IDD. Second, the rat caudal IVDs are different from the thoracic and lumbar IVDs in terms of mechanical loading, anatomy, dimensions, composition, and metabolism. In future studies, a comprehensive study of m6A modification changes in thoracic, lumbar and caudal IVDs at different ages would further scientifically explain the role of m6A modification in age-related IDD. In addition, whether the same pattern of m6A modification occurs in human aged IVD need further investigation. Third, the increased height of osseous endplate is known as an important feature for IDD. Since micro-CT was not adopted to detect the tails of rats, we didn't employ the height of osseous endplate as a degenerated feature in current study.

5 | CONCLUSIONS

In summary, we first comprehensively described the features and distributions of m6A modification in NP tissues of rats at different stages during the progression of NP aging. Our results showed the m6A peaks and m6A modified genes were closely related to the development of IDD, suggesting that m6A modification may play important roles in underlying mechanisms of IDD. These findings provide new insights for future studies, and may help explore novel targets for the treatment of degenerative disc related diseases.

AUTHOR CONTRIBUTIONS

Chencheng Feng, Shiwu Dong, and Yue Zhou conceived the project. Libangxi Liu, Hong Sun, and Yang Zhang designed experiments. Libangxi Liu, Hong Sun, and Yang Zhang performed the experiments and data analysis. Libangxi Liu and Hong Sun wrote the manuscript. Chang Liu, Miao Liu, Yong Zhuang, Xuezheng Ai, Dan Long, Bo Huang, and Changqing Li participated in the completion of the experiment and data analysis. All authors read and approved the final manuscript.

ACKNOWLEDGMENT

Not applicable.

FUNDING INFORMATION

This study was supported by National Natural Science Foundation of China (81902255, 81972114, 82072495), Natural Science Foundation of Chongqing in China (cstc2020jcyj-bshX0091, cstc2019jcyj-

msxmX0022), China Postdoctoral Science Foundation (2020M673652), Special Foundation of Army Military Medical University to enhance scientific and technological innovation ability (2020XQN15), Basic Research Program of Guizhou Science and Technology Department (QKH-ZK [2022] 430), Science and Technology Fund of Guizhou Provincial Health Commission (gzwjkj2019-1-133).

CONFLICT OF INTEREST STATEMENT

The authors declare that they have no competing interests.

DATA AVAILABILITY STATEMENT

All data generated or analyzed during this study are included in this published article and its supplementary information files. Meanwhile, the data that support the findings of this study are available from the corresponding author upon reasonable request. Transcriptome analysis and sequencing raw data have been stored in the Gene Expression Omnibus (GEO) database (<https://www.ncbi.nlm.nih.gov/>) GSE234369.

ETHICS STATEMENT

The protocol of animal experiments in current study was approved by the Animal Ethics Committee of Army Medical University (AMUWEC2020088).

ORCID

Chencheng Feng  <https://orcid.org/0000-0002-9393-304X>

REFERENCES

- Hadjipavlou AG, Tzermiadianos MN, Bogduk N, Zindrick MR. The pathophysiology of disc degeneration: a critical review. *J Bone Joint Surg Br*. 2008;90(10):1261-1270. doi:10.1302/0301-620X.90B10.20910
- Cieza A, Causey K, Kamenov K, Hanson SW, Chatterji S, Vos T. Global estimates of the need for rehabilitation based on the global burden of disease study 2019: a systematic analysis for the global burden of disease study 2019. *Lancet (London, England)*. 2021;396(10267):2006-2017. doi:10.1016/S0140-6736(20)32340-0
- Newell N, Little JP, Christou A, Adams MA, Adam CJ, Masouros SD. Biomechanics of the human intervertebral disc: a review of testing techniques and results. *J Mech Behav Biomed Mater*. 2017;69:420-434. doi:10.1016/j.jmbbm.2017.01.037
- Zhang GZ, Liu MQ, Chen HW, et al. NF-kappaB signalling pathways in nucleus pulposus cell function and intervertebral disc degeneration. *Cell Prolif*. 2021;54(7):e13057. doi:10.1111/cpr.13057
- Liao Z, Luo R, Li G, et al. Exosomes from mesenchymal stem cells modulate endoplasmic reticulum stress to protect against nucleus pulposus cell death and ameliorate intervertebral disc degeneration in vivo. *Theranostics*. 2019;9(14):4084-4100. doi:10.7150/thno.33638
- Sloan SR Jr, Wipplinger C, Kirnaz S, et al. Combined nucleus pulposus augmentation and annulus fibrosus repair prevents acute intervertebral disc degeneration after discectomy. *Sci Transl Med*. 2020;12(534):18-28. doi:10.1126/scitranslmed.aay2380
- He R, Wang Z, Cui M, et al. HIF1A alleviates compression-induced apoptosis of nucleus pulposus derived stem cells via upregulating autophagy. *Autophagy*. 2021;17(11):3338-3360. doi:10.1080/15548627.2021.1872227
- Cheng Z, Xiang Q, Wang J, Zhang Y. The potential role of melatonin in retarding intervertebral disc ageing and degeneration: a systematic review. *Ageing Res Rev*. 2021;70:101394. doi:10.1016/j.arr.2021.101394
- Cheung KM, Karppinen J, Chan D, et al. Prevalence and pattern of lumbar magnetic resonance imaging changes in a population study of one thousand forty-three individuals. *Spine (Phila Pa 1976)*. 2009;34(9):934-940. doi:10.1097/BRS.0b013e3181a01b3f
- Caldeira J, Santa C, Osorio H, et al. Matrisome profiling during intervertebral disc development and ageing. *Sci Rep*. 2017;7(1):11629. doi:10.1038/s41598-017-11960-0
- Chen PB, Shi GX, Liu T, et al. Oxidative stress aggravates apoptosis of nucleus pulposus cells through m(6)A modification of MAT2A pre-mRNA by METTL16. *Oxid Med Cell Longev*. 2022;2022:4036274. doi:10.1155/2022/4036274
- Wang Y, Che M, Xin J, Zheng Z, Li J, Zhang S. The role of IL-1beta and TNF-alpha in intervertebral disc degeneration. *Biomed Pharmacother*. 2020;131:110660. doi:10.1016/j.biopha.2020.110660
- Wang Y, Wang H, Zhuo Y, et al. SIRT1 alleviates high-magnitude compression-induced senescence in nucleus pulposus cells via PINK1-dependent mitophagy. *Aging*. 2020;12(16):16126-16141. doi:10.18632/aging.103587
- Yin X, Motorwala A, Vesvoranan O, Levene HB, Gu W, Huang CY. Effects of glucose deprivation on ATP and proteoglycan production of intervertebral disc cells under hypoxia. *Sci Rep*. 2020;10(1):8899. doi:10.1038/s41598-020-65691-w
- Feng C, Liu H, Yang M, Zhang Y, Huang B, Zhou Y. Disc cell senescence in intervertebral disc degeneration: causes and molecular pathways. *Cell Cycle*. 2016;15(13):1674-1684. doi:10.1080/15384101.2016.1152433
- Clouet J, Pot-Vaucel M, Grimandi G, et al. Characterization of the age-dependent intervertebral disc changes in rabbit by correlation between MRI, histology and gene expression. *BMC Musculoskelet Disord*. 2011;12:147. doi:10.1186/1471-2474-12-147
- Silwal P, Nguyen-Thai AM, Mohammad HA, et al. Cellular senescence in intervertebral disc aging and degeneration: molecular mechanisms and potential therapeutic opportunities. *Biomolecules*. 2023;13(4):686. doi:10.3390/biom13040686
- Che H, Li J, Li Y, et al. p16 deficiency attenuates intervertebral disc degeneration by adjusting oxidative stress and nucleus pulposus cell cycle. *Elife*. 2020;9:1-23. doi:10.7554/eLife.52570
- Patil P, Dong Q, Wang D, et al. Systemic clearance of p16(INK4a)-positive senescent cells mitigates age-associated intervertebral disc degeneration. *Aging Cell*. 2019;18(3):e12927. doi:10.1111/accel.12927
- Li G, Luo R, Zhang W, et al. m6A hypomethylation of DNMT3B regulated by ALKBH5 promotes intervertebral disc degeneration via E4F1 deficiency. *Clin Transl Med*. 2022;12(3):e765. doi:10.1002/ctm2.765
- Liu C, Liu L, Yang M, et al. A positive feedback loop between EZH2 and NOX4 regulates nucleus pulposus cell senescence in age-related intervertebral disc degeneration. *Cell Div*. 2020;15:2. doi:10.1186/s13008-020-0060-x
- Li G, Ma L, He S, et al. WTAP-mediated m(6)A modification of lncRNA NORAD promotes intervertebral disc degeneration. *Nat Commun*. 2022;13(1):1469. doi:10.1038/s41467-022-28990-6
- Fu Y, Dominissini D, Rechavi G, He C. Gene expression regulation mediated through reversible m(6)A RNA methylation. *Nat Rev Genet*. 2014;15(5):293-306. doi:10.1038/nrg3724
- Desrosiers R, Friderici K, Rottman F. Identification of methylated nucleosides in messenger RNA from Novikoff hepatoma cells. *Proc Natl Acad Sci U S A*. 1974;71(10):3971-3975. doi:10.1073/pnas.71.10.3971
- Wang S, Lv W, Li T, et al. Dynamic regulation and functions of mRNA m6A modification. *Cancer Cell Int*. 2022;22(1):48. doi:10.1186/s12935-022-02452-x
- Jiang X, Liu B, Nie Z, et al. The role of m6A modification in the biological functions and diseases. *Signal Transduct Target Ther*. 2021;6(1):74. doi:10.1038/s41392-020-00450-x
- Li G, Song Y, Liao Z, et al. Bone-derived mesenchymal stem cells alleviate compression-induced apoptosis of nucleus pulposus cells by N6

- methyladenosine of autophagy. *Cell Death Dis.* 2020;11(2):103. doi:[10.1038/s41419-020-2284-8](https://doi.org/10.1038/s41419-020-2284-8)
28. He S, Zhang Y, Zhou Z, et al. Similarity and difference between aging and puncture-induced intervertebral disc degeneration. *J Orthop Res.* 2022;40:2565-2575. doi:[10.1002/jor.25281](https://doi.org/10.1002/jor.25281)
 29. Pfirrmann CW, Metzdorf A, Zanetti M, Hodler J, Boos N. Magnetic resonance classification of lumbar intervertebral disc degeneration. *Spine (Phila Pa 1976).* 2001;26(17):1873-1878. doi:[10.1097/00007632-200109010-00011](https://doi.org/10.1097/00007632-200109010-00011)
 30. Caprez S, Menzel U, Li Z, Grad S, Alini M, Peroglio M. Isolation of high-quality RNA from intervertebral disc tissue via pronase predigestion and tissue pulverization. *JOR Spine.* 2018;1(2):e1017. doi:[10.1002/jsp2.1017](https://doi.org/10.1002/jsp2.1017)
 31. Feng C, Zhang Y, Yang M, et al. Oxygen-sensing Nox4 generates genotoxic ROS to induce premature senescence of nucleus pulposus cells through MAPK and NF-kappaB pathways. *Oxid Med Cell Longev.* 2017;2017:7426458. doi:[10.1155/2017/7426458](https://doi.org/10.1155/2017/7426458)
 32. Liu L, Zhang Y, Fu J, et al. Gli1 depletion induces oxidative stress and apoptosis of nucleus pulposus cells via Fos in intervertebral disc degeneration. *J Orthop Translat.* 2023;40:116-131. doi:[10.1016/j.jot.2023.05.008](https://doi.org/10.1016/j.jot.2023.05.008)
 33. Lai A, Gansau J, Gullbrand SE, et al. Development of a standardized histopathology scoring system for intervertebral disc degeneration in rat models: an initiative of the ORS spine section. *JOR Spine.* 2021;4(2):e1150. doi:[10.1002/jsp2.1150](https://doi.org/10.1002/jsp2.1150)
 34. Liao Z, Su D, Liu H, et al. Dihydroartemisinin attenuated intervertebral disc degeneration via inhibiting PI3K/AKT and NF-kappaB signaling pathways. *Oxid Med Cell Longev.* 2022;2022:8672969. doi:[10.1155/2022/8672969](https://doi.org/10.1155/2022/8672969)
 35. Zhang HJ, Liao HY, Bai DY, Wang ZQ, Xie XW. MAPK /ERK signaling pathway: a potential target for the treatment of intervertebral disc degeneration. *Biomed Pharmacother.* 2021;143:112170. doi:[10.1016/j.biopha.2021.112170](https://doi.org/10.1016/j.biopha.2021.112170)
 36. Chen CC, Chen J, Wang WL, Xie L, Shao CQ, Zhang YX. Inhibition of the P53/P21 pathway attenuates the effects of senescent nucleus pulposus cell-derived exosomes on the senescence of nucleus pulposus cells. *Orthop Surg.* 2021;13(2):583-591. doi:[10.1111/os.12886](https://doi.org/10.1111/os.12886)
 37. Alvarez-Garcia O, Matsuzaki T, Olmer M, et al. FOXO are required for intervertebral disk homeostasis during aging and their deficiency promotes disk degeneration. *Aging Cell.* 2018;17(5):e12800. doi:[10.1111/acer.12800](https://doi.org/10.1111/acer.12800)
 38. Zhang T, Zhang SW, Zhang SY, Gao SJ, Chen Y, Huang Y. m6A-express: uncovering complex and condition-specific m6A regulation of gene expression. *Nucleic Acids Res.* 2021;49(20):e116. doi:[10.1093/nar/gkab714](https://doi.org/10.1093/nar/gkab714)
 39. Xiang H, Yan F, Liu H. The genetic association identified between intervertebral disc degeneration and associated risk factors based on a systems biology approach. *Spine (Phila Pa 1976).* 2022;47(8):E370-E384. doi:[10.1097/BRS.00000000000004312](https://doi.org/10.1097/BRS.00000000000004312)
 40. Zhao X, Shen P, Li H, et al. Carbonic anhydrase 12 protects endplate cartilage from degeneration regulated by IGF-1/PI3K/CREB signaling pathway. *Front Cell Dev Biol.* 2020;8:595969. doi:[10.3389/fcell.2020.595969](https://doi.org/10.3389/fcell.2020.595969)
 41. Vo NV, Hartman RA, Yurube T, Jacobs LJ, Sowa GA, Kang JD. Expression and regulation of metalloproteinases and their inhibitors in intervertebral disc aging and degeneration. *Spine J.* 2013;13(3):331-341. doi:[10.1016/j.spinee.2012.02.027](https://doi.org/10.1016/j.spinee.2012.02.027)
 42. Han J, Kong H, Wang X, Zhang XA. Novel insights into the interaction between N6-methyladenosine methylation and noncoding RNAs in musculoskeletal disorders. *Cell Prolif.* 2022;55(10):e13294. doi:[10.1111/cpr.13294](https://doi.org/10.1111/cpr.13294)
 43. Jiang C, Chen Z, Wang X, et al. The potential mechanisms and application prospects of non-coding RNAs in intervertebral disc degeneration. *Front Endocrinol (Lausanne).* 2022;13:1081185. doi:[10.3389/fendo.2022.1081185](https://doi.org/10.3389/fendo.2022.1081185)
 44. Wang F, Cai F, Shi R, Wang XH, Wu XT. Aging and age related stresses: a senescence mechanism of intervertebral disc degeneration. *Osteoarthritis Cartil.* 2016;24(3):398-408. doi:[10.1016/j.joca.2015.09.019](https://doi.org/10.1016/j.joca.2015.09.019)
 45. Tang X, Jing L, Chen J. Changes in the molecular phenotype of nucleus pulposus cells with intervertebral disc aging. *PLoS One.* 2012;7(12):e52020. doi:[10.1371/journal.pone.0052020](https://doi.org/10.1371/journal.pone.0052020)
 46. Zhu H, Sun B, Zhu L, Zou G, Shen Q. N6-Methyladenosine induced miR-34a-5p promotes TNF- α -induced nucleus pulposus cell senescence by targeting SIRT1. *Front Cell Dev Biol.* 2021;9:642437. doi:[10.3389/fcell.2021.642437](https://doi.org/10.3389/fcell.2021.642437)
 47. Yuan X, Li T, Shi L, Miao J, Guo Y, Chen YA-O. Human umbilical cord mesenchymal stem cells deliver exogenous miR-26a-5p via exosomes to inhibit nucleus pulposus cell pyroptosis through METTL14/NLRP3. *Mol Med.* 2021;27(1):91. doi:[10.1186/s10020-021-00355-7](https://doi.org/10.1186/s10020-021-00355-7)
 48. Xiao L, Hu B, Ding B, et al. N(6)-methyladenosine RNA methyltransferase like 3 inhibits extracellular matrix synthesis of endplate chondrocytes by downregulating sex-determining region Y-box transcription factor 9 expression under tension. *Osteoarthritis Cartil.* 2022;30(4):613-625. doi:[10.1016/j.joca.2022.01.002](https://doi.org/10.1016/j.joca.2022.01.002)
 49. Zhu B, Chen HX, Li S, et al. Comprehensive analysis of N6-methyladenosine (m6A) modification during the degeneration of lumbar intervertebral disc in mice. *J Orthop Translat.* 2021;31:126-138. doi:[10.1016/j.jot.2021.10.008](https://doi.org/10.1016/j.jot.2021.10.008)
 50. Castro-Hernandez R, Berulava T, Metelova M, et al. Conserved reduction of m(6)A RNA modifications during aging and neurodegeneration is linked to changes in synaptic transcripts. *Proc Natl Acad Sci U S A.* 2023;120(9):e2204933120. doi:[10.1073/pnas.2204933120](https://doi.org/10.1073/pnas.2204933120)
 51. Chen X, Yu C, Guo M, et al. Down-regulation of m6A mRNA methylation is involved in dopaminergic neuronal death. *ACS Chem Neurosci.* 2019;10(5):2355-2363. doi:[10.1021/acschemneuro.8b00657](https://doi.org/10.1021/acschemneuro.8b00657)
 52. Shafik AM, Zhang F, Guo Z, et al. N6-methyladenosine dynamics in neurodevelopment and aging, and its potential role in Alzheimer's disease. *Genome Biol.* 2021;22(1):17. doi:[10.1186/s13059-020-02249-z](https://doi.org/10.1186/s13059-020-02249-z)
 53. Yang Y, Hsu PJ, Chen YS, Yang YG. Dynamic transcriptomic m(6)A decoration: writers, erasers, readers and functions in RNA metabolism. *Cell Res.* 2018;28(6):616-624. doi:[10.1038/s41422-018-0040-8](https://doi.org/10.1038/s41422-018-0040-8)
 54. He PC, Wei J, Dou X, et al. Exon architecture controls mRNA m(6)A suppression and gene expression. *Science.* 2023;379(6633):677-682. doi:[10.1126/science.abj9090](https://doi.org/10.1126/science.abj9090)
 55. Sun J, Cheng B, Su Y, et al. The potential role of m6A RNA methylation in the aging process and aging-associated diseases. *Front Genet.* 2022;13:869950. doi:[10.3389/fgene.2022.869950](https://doi.org/10.3389/fgene.2022.869950)
 56. Chen L, Zhang C, Ma W, Huang J, Zhao Y, Liu H. METTL3-mediated m6A modification stabilizes TERRA and maintains telomere stability. *Nucleic Acids Res.* 2022;50(20):11619-11634. doi:[10.1093/nar/gkac1027](https://doi.org/10.1093/nar/gkac1027)
 57. Xu Z, Qiu P, Jiang Y, et al. m6A modification mediates endothelial cell responses to oxidative stress in vascular aging induced by low fluid shear stress. *Oxid Med Cell Longev.* 2023;2023:8134027. doi:[10.1155/2023/8134027](https://doi.org/10.1155/2023/8134027)
 58. Wu Z, Shi Y, Lu M, et al. METTL3 counteracts premature aging via m6A-dependent stabilization of MIS12 mRNA. *Nucleic Acids Res.* 2020;48(19):11083-11096. doi:[10.1093/nar/gkaa816](https://doi.org/10.1093/nar/gkaa816)
 59. NaPier Z, Kanim LEA, Arabi Y, et al. Omega-3 fatty acid supplementation reduces intervertebral disc degeneration. *Med Sci Monit.* 2019;25:9531-9537. doi:[10.12659/MSM.918649](https://doi.org/10.12659/MSM.918649)
 60. Yi YY, Chen H, Zhang SB, Xu HW, Fang XY, Wang SJ. Exogenous klotho ameliorates extracellular matrix degradation and angiogenesis in intervertebral disc degeneration via inhibition of the Rac1/PAK1/MMP-2 signaling axis. *Mech Ageing Dev.* 2022;207:111715. doi:[10.1016/j.mad.2022.111715](https://doi.org/10.1016/j.mad.2022.111715)
 61. Hu R, Wang MQ, Ni SH, et al. Salidroside ameliorates endothelial inflammation and oxidative stress by regulating the AMPK/NF-

- kappaB/NLRP3 signaling pathway in AGEs-induced HUVECs. *Eur J Pharmacol.* 2020;867:172797. doi:[10.1016/j.ejphar.2019.172797](https://doi.org/10.1016/j.ejphar.2019.172797)
62. Hou T, Sun X, Zhu J, et al. IL-37 ameliorating allergic inflammation in atopic dermatitis through regulating microbiota and AMPK-mTOR signaling pathway-modulated autophagy mechanism. *Front Immunol.* 2020;11:752. doi:[10.3389/fimmu.2020.00752](https://doi.org/10.3389/fimmu.2020.00752)
 63. Li X, Li C, Zhang W, Wang Y, Qian P, Huang H. Inflammation and aging: signaling pathways and intervention therapies. *Signal Transduct Target Ther.* 2023;8(1):239. doi:[10.1038/s41392-023-01502-8](https://doi.org/10.1038/s41392-023-01502-8)
 64. Chen HW, Zhou JW, Zhang GZ, Luo ZB, Li L, Kang XW. Emerging role and therapeutic implication of mTOR signalling in intervertebral disc degeneration. *Cell Prolif.* 2023;56(1):e13338. doi:[10.1111/cpr.13338](https://doi.org/10.1111/cpr.13338)
 65. Lin J, Zhuge J, Zheng X, et al. Urolithin A-induced mitophagy suppresses apoptosis and attenuates intervertebral disc degeneration via the AMPK signaling pathway. *Free Radic Biol Med.* 2020;150:109-119. doi:[10.1016/j.freeradbiomed.2020.02.024](https://doi.org/10.1016/j.freeradbiomed.2020.02.024)
 66. Yurube T, Ito M, Kakiuchi Y, Kuroda R, Kakutani K. Autophagy and mTOR signaling during intervertebral disc aging and degeneration. *JOR Spine.* 2020;3(1):e1082. doi:[10.1002/jsp2.1082](https://doi.org/10.1002/jsp2.1082)
 67. Yang Q, Guo XP, Cheng YL, Wang Y. MicroRNA-143-5p targeting eEF2 gene mediates intervertebral disc degeneration through the AMPK signaling pathway. *Arthritis Res Ther.* 2019;21(1):97. doi:[10.1186/s13075-019-1863-5](https://doi.org/10.1186/s13075-019-1863-5)
 68. Zhao BS, Roundtree IA, He C. Post-transcriptional gene regulation by mRNA modifications. *Nat Rev Mol Cell Biol.* 2017;18(1):31-42. doi:[10.1038/nrm.2016.132](https://doi.org/10.1038/nrm.2016.132)
 69. Li J, Chen K, Dong X, et al. YTHDF1 promotes mRNA degradation via YTHDF1-AGO2 interaction and phase separation. *Cell Prolif.* 2022; 55(1):e13157. doi:[10.1111/cpr.13157](https://doi.org/10.1111/cpr.13157)
 70. Hou G, Zhao X, Li L, et al. SUMOylation of YTHDF2 promotes mRNA degradation and cancer progression by increasing its binding affinity with m6A-modified mRNAs. *Nucleic Acids Res.* 2021;49(5):2859-2877. doi:[10.1093/nar/gkab065](https://doi.org/10.1093/nar/gkab065)
 71. Huang H, Weng H, Sun W, et al. Recognition of RNA N(6)-methyladenosine by IGF2BP proteins enhances mRNA stability and translation. *Nat Cell Biol.* 2018;20(3):285-295. doi:[10.1038/s41556-018-0045-z](https://doi.org/10.1038/s41556-018-0045-z)
 72. Yu D, Pan M, Li Y, et al. RNA N6-methyladenosine reader IGF2BP2 promotes lymphatic metastasis and epithelial-mesenchymal transition of head and neck squamous carcinoma cells via stabilizing slug mRNA in an m6A-dependent manner. *J Exp Clin Cancer Res.* 2022;41(1):6. doi:[10.1186/s13046-021-02212-1](https://doi.org/10.1186/s13046-021-02212-1)
 73. Zhang N, Shen Y, Li H, et al. The m6A reader IGF2BP3 promotes acute myeloid leukemia progression by enhancing RCC2 stability. *Exp Mol Med.* 2022;54(2):194-205. doi:[10.1038/s12276-022-00735-x](https://doi.org/10.1038/s12276-022-00735-x)

SUPPORTING INFORMATION

Additional supporting information can be found online in the Supporting Information section at the end of this article.

How to cite this article: Liu L, Sun H, Zhang Y, et al. Dynamics of N6-methyladenosine modification during aging and their potential roles in the degeneration of intervertebral disc. *JOR Spine.* 2024;7(1):e1316. doi:[10.1002/jsp2.1316](https://doi.org/10.1002/jsp2.1316)